

Convex Relaxations and Approximations of Chance-Constrained AC-OPF Problems

Lejla Halilbašić, *Student Member, IEEE*, Pierre Pinson, *Senior Member, IEEE*,
and Spyros Chatzivasileiadis, *Member, IEEE*

Abstract—This paper deals with the impact of linear approximations for the unknown nonconvex confidence region of chance-constrained AC optimal power flow problems. Such approximations are required for the formulation of tractable chance constraints. In this context, we introduce the first formulation of a chance-constrained second-order cone (SOC) OPF. The proposed formulation provides convergence guarantees due to its convexity, while it demonstrates high computational efficiency. Combined with an AC feasibility recovery, it is able to identify better solutions than chance-constrained nonconvex AC-OPF formulations. To the best of our knowledge, this paper is the first to perform a rigorous analysis of the AC feasibility recovery procedures for robust SOC-OPF problems. We identify the issues that arise from the linear approximations, and by using a reformulation of the quadratic chance constraints related to the apparent power flow, we introduce new parameters that are able to reshape the approximation of the confidence region, offering a high degree of flexibility.

Index Terms—Chance-constrained AC-OPF, convex relaxations, second order cone programming, AC feasibility recovery.

I. INTRODUCTION

WHILE power system operations are increasingly relying on the AC Optimal Power Flow (OPF) to identify optimal decisions, higher shares of intermittent renewable generation add an additional layer of complexity, calling for modeling approaches which account for uncertainty. Literature considers uncertainty either in the form of stochastic formulations, which optimizes over several possible realizations (i.e. scenario-based), or in the form of robust formulations, where chance constraints are incorporated in the optimization problem accounting for a continuous range of uncertainty. This paper focuses on chance-constrained optimization.

As the AC-OPF is a nonlinear and nonconvex problem, it is impossible to formulate tractable chance constraints able to cover the whole continuous uncertainty space. Instead, literature has proposed tractable approximations. Recent research in [1]–[4] has focused on developing formulations of the chance-constrained AC-OPF based on partial linearizations. Ref. [1]–[3] focus on the original AC-OPF formulation, while in previous work [4] we additionally introduce convex relaxations of the AC power flow equations based on semidefinite programming (SDP).

Chance constraints define the maximum allowable violation probability ϵ of inequality constraints and reduce the nonconvex feasible space of the AC-OPF to a desired confidence

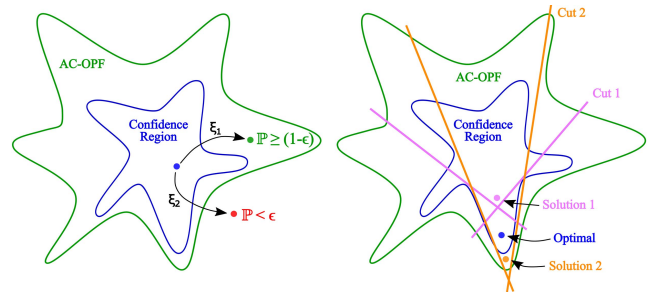


Fig. 1. Left: Illustration of the feasible space of the AC-OPF and the chance-constrained AC-OPF (confidence region). Right: Illustration of the approximation of the confidence region using linear cuts.

region, which is also nonconvex as depicted in blue in Fig. 1. This confidence region includes only operating points which under any realization of the uncertainty ξ are guaranteed to remain within the feasible space of the original AC-OPF (in green in Fig. 1) with a probability of at least $(1 - \epsilon)$.

The main challenge of the chance-constrained AC-OPF lies in approximating the unknown nonconvex confidence region. Common to all approaches in [1]–[4] is that they approximate the impact of the uncertainty by a linearization allowing to reformulate the chance constraints to tractable deterministic constraints. These are tighter than the original constraints and represent linear cuts to the original feasible space in order to approximate the confidence region. As visualized in Fig. 1, depending on the quality of the cuts the identified operating points may either lie outside the confidence region (solution 2) [1] or are too conservative (solution 1). The authors in [1], [2] develop an iterative framework for approximating the chance-constrained AC-OPF by alternating between an AC-OPF and a computation of the constraint tightenings (i.e., the linear cuts) based on a first-order Taylor series expansion around the forecasted operating point. Due to the nonconvex nature of the AC-OPF, however, the algorithm is not guaranteed to converge. The SDP relaxation of the chance-constrained AC-OPF developed in [4] improves on the approximation of the confidence region by optimizing over affine control policies and aims at providing AC feasible solutions and global optimality guarantees. However, as SDP solvers are still under development it can be computationally challenging.

This paper focuses on second-order cone relaxations (SOC) of the AC-OPF as a good trade-off between approaches for two reasons. First, compared with the original AC-OPF formulation, SOC relaxations define a convex problem which is guaranteed to converge. Second, SOC relaxations are computationally more efficient than SDP relaxations. It must be noted that compared to SDP, SOC relaxations provide a less tight

This work is supported by the EU project BEST PATHS, Grant No. 612748. L. Halilbašić, P. Pinson, and S. Chatzivasileiadis are with the Department of Electrical Engineering, Technical University of Denmark, Kongens Lyngby, Denmark. email: {lhal, ppin, spchatz}@elektro.dtu.dk

relaxation, and require strengthening [5] or other procedures to recover an AC feasible point. Such procedures are often necessary in the SDP formulation as well though.

SOC-OPF algorithms considering uncertainty have been proposed in [6]–[8], where the authors develop convex formulations of the robust two-stage AC-OPF problem focusing on the worst-case uncertainty realization. Specifically, in [7] and [8] SOC relaxations are used within the framework of an affinely adjustable robust OPF (first proposed in [9] for a DC-OPF). However, both papers consider only affine policies for active power generation neglecting the impact of the uncertainty on all other control and state variables. A very extensive framework for relaxations of robust AC-OPFs is provided in [6], where the authors develop three methods using conic duality to obtain tractable formulations of the robust AC-OPF based on SOC-, SDP-, and DC-OPFs. To guarantee AC feasible solutions, the conic OPF models are used to approximate the second stage of the two-stage robust optimization problem and are then solved alternately with an AC-OPF, which represents the first stage problem. However, as in [1] this results in a nonconvex iterative program, which is not guaranteed to converge. None of the papers mentioned address the issue of AC infeasibility of the SOC-OPF solutions.

The main contributions of this work are:

- the first formulation of a chance-constrained SOC-OPF (CC-SOC-OPF), able to provide both convergence guarantees and high computational efficiency; coupled with an AC feasibility recovery it identifies better solutions than the chance-constrained nonconvex AC-OPF formulation
- the approximation of quadratic apparent power flow chance constraints with linear chance constraints using results proposed in [10]
- the introduction of new parameters able to reshape the approximation of the confidence region, along with a rigorous analysis of the linear approximations; these parameters offer a high degree of flexibility for the robustness of the solution.

The remainder of this paper is organized as follows: Section II introduces the SOC relaxation of the AC-OPF, while Section III focuses on the formulation of the CC-SOC-OPF. Results from a case study are presented in Section IV. Section V concludes.

II. AC-OPF REFORMULATIONS AND RELAXATIONS

The AC-OPF is a nonlinear and nonconvex optimization problem, which aims at determining the least-cost, optimal generation dispatch satisfying all demand under consideration of generator active and reactive power, line flow and nodal voltage magnitude limits [11]. It is commonly defined in the space of $\mathbf{x} := \{\mathbf{P}, \mathbf{Q}, \mathbf{V}, \theta\}$ variables, which are defined per node and represent active power injections, reactive power injections, voltage magnitudes and voltage angles, respectively. Thus, set \mathbf{x} consists of $4|\mathcal{N}|$ optimization variables, where \mathcal{N} denotes the set of network nodes. Bold letters indicate vectors or matrices.

Alternatively, the AC-OPF can be represented using an extended and modified set of optimization variables of size $(4|\mathcal{N}| + 2|\mathcal{L}|)$ [5], [12], [13], where \mathcal{L} denotes the set of lines (i.e., network edges). New variables are introduced to

capture the nonlinearities and nonconvexities of the AC power flow equations: (a) $u_i := V_i^2$, (b) $c_l := V_i V_j \cos(\theta_{ij})$ and (c) $s_l := -V_i V_j \sin(\theta_{ij})$, where each transmission line $l \in \mathcal{L}$ is associated with a tuple (i, j) defining its sending and receiving node. As a result, the AC-OPF is transformed from the space of $\mathbf{x} := \{\mathbf{P}, \mathbf{Q}, \mathbf{V}, \theta\}$ variables to the space of $\mathbf{y} := \{\mathbf{P}, \mathbf{Q}, \mathbf{u}, \theta, \mathbf{c}, \mathbf{s}\}$ variables and is given by

$$\min_{\mathbf{y}} \sum_{i \in \mathcal{G}} c_i^G \left(P_i^G \right) \quad (1)$$

$$\text{s.t. } P_i = G_{ii} u_i + \sum_{l=(i,j)} \left(G_{ij} c_l - B_{ij} s_l \right) + \sum_{l=(j,i)} \left(G_{ij} c_l + B_{ij} s_l \right), \quad \forall i \in \mathcal{N} \quad (2)$$

$$Q_i = -B_{ii} u_i - \sum_{l=(i,j)} \left(B_{ij} c_l + G_{ij} s_l \right) - \sum_{l=(j,i)} \left(G_{ij} c_l - B_{ij} s_l \right), \quad \forall i \in \mathcal{N} \quad (3)$$

$$0 = c_l^2 + s_l^2 - u_i u_j, \quad \forall l \in \mathcal{L}, \quad (4)$$

$$0 = \theta_j - \theta_i - \text{atan}\left(\frac{s_l}{c_l}\right), \quad \forall l \in \mathcal{L}, \quad (5)$$

$$S_{ij}^2 \leq (\overline{S_l})^2, \quad S_{ji}^2 \leq (\overline{S_l})^2, \quad \forall l \in \mathcal{L}, \quad (6)$$

$$\underline{V}_i^2 \leq u_i \leq \overline{V}_i^2, \quad \forall i \in \mathcal{N}, \quad (7)$$

$$\underline{P}_i^G \leq P_i^G \leq \overline{P}_i^G, \quad \underline{Q}_i^G \leq Q_i^G \leq \overline{Q}_i^G, \quad \forall i \in \mathcal{G}, \quad (8)$$

$$-\overline{V}_i \overline{V}_j \leq c_l, s_l \leq \overline{V}_i \overline{V}_j, \quad \forall l \in \mathcal{L}, \quad (9)$$

$$\theta_{ref} = 0. \quad (10)$$

The objective function (1) minimizes active power generation costs. Superscript G denotes the contribution of conventional generators to the power injection P_i and Q_i at node i (summarized in vectors \mathbf{P} and \mathbf{Q} for all nodes), while $\mathcal{G} \subseteq \mathcal{N}$ contains only nodes, which have conventional generators connected to them. Constraints (2) and (3) represent nodal active and reactive power balance equations, respectively. Equation (4) arises from the variable transformation, while voltage angles are reintroduced through constraint (5). The latter can be omitted for radial networks. Constraints (7)–(9) limit the decision variables within their upper and lower bounds. The two inequalities in (6) constrain the apparent power flow in both directions of the line, where S_{ij}^2 (and analogously S_{ji}^2) is defined as

$$\begin{aligned} S_{ij}^2 &= P_{ij}^2 + Q_{ij}^2 \\ &= \left(-G_{ij} u_i + G_{ij} c_l - B_{ij} s_l \right)^2 \\ &\quad + \left((B_{ij} - B_{ij}^{sh}) u_i - B_{ij} c_l - G_{ij} s_l \right)^2, \quad \forall l \in \mathcal{L}. \end{aligned} \quad (11)$$

Note that we assume a π -model of the transmission line with reactive shunt elements B_{ij}^{sh} only. Equation (10) sets the voltage angle of the reference bus to zero.

The optimization problem (1)–(10) is an exact reformulation of the original AC-OPF and still nonlinear and nonconvex. However, when relaxing constraints (4) and (5), the original AC-OPF can be approximated by a convex quadratic optimization problem, which can be solved to global optimality. To this end, equation (4) is replaced by its convex second-order cone representation: $c_{ij}^2 + s_{ij}^2 \leq u_i u_j$, while (5) can

be linearized using a Taylor series expansion as proposed in [13] resulting in an iterative conic algorithm. The convergence is determined by the change in \mathbf{c} and \mathbf{s} variables, e.g., $\|\mathbf{c}^\nu - \mathbf{c}^{\nu-1}\|_\infty$. Alternative convex approximations to (5) have also been proposed in [5]. We refer to the relaxed OPF as *Second-Order Cone OPF* (SOC-OPF). Note that (6) is already a convex second-order cone constraint and does not need to be reformulated. Given that the SOC-OPF is a relaxation of the AC-OPF, identified solutions might not be feasible to the original problem. We address this issue in Section III, where we propose an ex post AC feasibility recovery based on an AC power flow analysis, while in Section IV we demonstrate in our case study how the proposed procedure is not only able to recover the AC-OPF solution of a nonlinear solver but can also identify better solutions.

III. PROBABILISTIC OPTIMAL POWER FLOW

The chance-constrained OPF restricts the feasible space to a desired confidence region (CR) and identifies optimal decisions for the forecasted operating point, such that for any realization of the uncertainty and appropriate remedial actions all constraints are satisfied with a desired probability. Remedial or corrective control actions can be either pre-determined or embedded as optimization variables in the chance-constrained OPF.

A. Chance-constrained SOC Optimal Power Flow

In this paper, we propose the first formulation of a CC-SOC-OPF, which avoids the nonconvexities and convergence issues of the chance-constrained AC-OPF [1] and can be computationally more efficient than other convex formulations of chance-constrained AC-OPF problems [4]. Similar to the literature, we assume wind power generation $\tilde{\mathbf{P}}^W$ to be the only source of uncertainty. The actual wind realization \tilde{P}_i^W is modeled as the sum of forecasted value P_i^W and deviation ξ_i ,

$$\tilde{P}_i^W = P_i^W + \xi_i, \quad \forall i \in \mathcal{W}. \quad (12)$$

$\mathcal{W} \subseteq \mathcal{N}$ denotes the set of nodes containing wind generators, while superscript W refers to the contribution of wind power to the nodal power injection at node i . Recently, grid codes also require renewable energy generators to be able to provide reactive power [14]. We include the reactive power generation of wind farms \mathbf{Q}^W as optimization variables and allow for exchange of reactive power according to a pre-defined power factor $\cos \phi$.

We model all decision variables $\tilde{\mathbf{y}}(\xi)$ of the OPF as functions of the uncertainty ξ : $\tilde{\mathbf{y}}(\xi) = \mathbf{y} + \Delta\mathbf{y}(\xi)$, where \mathbf{y} and $\Delta\mathbf{y}(\xi)$ represent the optimal setpoint at the forecasted operating point and the system response to a change in active power injection (i.e., wind power deviation ξ), respectively. The chance-constrained OPF minimizes the total generation cost for the forecasted operating point and is formulated as follows

$$\min_{\mathbf{y}} \sum_{i \in \mathcal{G}} c_i^G (P_i^G) \quad (13)$$

$$\text{s.t. (2) - (5), (10) for } \tilde{\mathbf{y}} = \mathbf{y}, \quad (14)$$

$$\mathbb{P}\left\{ \text{(6) - (9)} \right\} \geq 1 - \epsilon \quad \text{for } \tilde{\mathbf{y}} = \mathbf{y} + \Delta\mathbf{y}(\xi), \quad (15)$$

where $\epsilon \in (0, 1)$ represents the allowed constraint violation probability. Thus, the CR (i.e., the restricted feasible space) of the chance-constrained OPF is defined by the confidence level $(1 - \epsilon)$. Problem (13)-(15) represents the chance-constrained formulation of the exact AC-OPF (1)-(10) and can be relaxed as described in Section II to obtain the convex CC-SOC-OPF. All equality constraints (2)-(5) and relaxations of them are considered for the forecasted operating point only, as including (12) and $\tilde{\mathbf{y}}(\xi)$ directly in (14) would render the problem semi-infinite and thus, intractable.

B. Control Policies: Modeling the System Response

In order to approximately model the system response to a change in wind power injection ξ , we use linear policies for all variables concerned.

1) *Reserve Deployment*: Fluctuations in active power generation are balanced by conventional generators, which are assumed to provide up- and down-reserves according to their generator participation factors γ . The participation factors are pre-determined and proportional to each generator's installed capacity with respect to the total system installed capacity. The generator output is adjusted according to the total power mismatch $\Xi = \sum_{i \in \mathcal{W}} \xi_i$ [15]. Hence, the sum of all generator contributions to the reserve deployment needs to balance the total power mismatch Ξ , which implies the following condition: $\sum_{i \in \mathcal{G}} \gamma_i = 1$, so that the total contribution of all generators equals the total power mismatch $\sum_{i \in \mathcal{G}} \gamma_i \sum_{i \in \mathcal{W}} \xi_i = \Xi$. Note that the participation factors can also be included as optimization variables and defined for each wind infeed individually. However, a higher number of optimization variables and additional second-order cone constraints in case of the latter also increase the computational burden. Apart from balancing the total active power mismatch, we also need to account for the nonlinear changes in transmission losses, apparent power flows and all remaining decision variables $\mathbf{y} \setminus \mathbf{P}$ due to variations in wind infeed.

2) *Linear Decision Rules*: To this end, we derive linear sensitivities of each variable with respect to the uncertainty based on a Taylor series expansion around the forecasted operating point. We model the response as follows: $\Delta\mathbf{y}(\xi) = \frac{\partial \mathbf{y}}{\partial \xi} \xi = \mathbf{Y}\xi$, such that $\tilde{\mathbf{y}}(\xi)$ represents a linear decision rule (LDR) with respect to the uncertainty. The authors in [1], [2], [16] have derived the linear sensitivity factors from the Jacobian matrix at the forecasted operating point of the original AC power flow equations. The detailed derivation can be found in [17]. In this work, we derive the linear sensitivity factors \mathbf{Y} based on the Jacobian matrix of the alternative load flow equations (2)-(5), such that we can directly use them as input to the convex chance-constrained SOC-OPF:

$$\begin{bmatrix} \Delta\mathbf{P} \\ \Delta\mathbf{Q} \\ \mathbf{0} \\ \mathbf{0} \end{bmatrix} = [\mathbf{J}^{\text{SOC}}] \Big|_{\mathbf{y}} \begin{bmatrix} \Delta\mathbf{u} \\ \Delta\mathbf{c} \\ \Delta\mathbf{s} \\ \Delta\theta \end{bmatrix}. \quad (16)$$

The left-hand side of equation (16) can also be expressed in terms of the uncertain wind infeed, the generator participation factors, the optimal ratio between reactive and active wind power generation at the forecasted operating point and the unknown nonlinear changes in active and reactive power.

We replace the entries for $\Delta \mathbf{P}$ and $\Delta \mathbf{Q}$ accordingly and reduce the system of equations considering the following assumptions, which are aligned with current practices in power system operations:

- the change in active power losses is compensated by the generator at the reference bus: $\Delta \mathbf{P}_{\text{PV}, \text{PQ}}^{\text{loss}} = \mathbf{0}$;
- changes in reactive power generation are compensated by generators at PV and reference buses, as PQ buses are assumed to keep their active and reactive power injection constant: $\Delta \mathbf{Q}_{\text{PQ}}^{\text{G}} = \mathbf{0}$;
- generators at PV and reference buses regulate their reactive power output to keep the voltage magnitude and thus, the square of the voltage magnitude constant: $\Delta \mathbf{u}_{\text{PV}, \text{ref}} = \mathbf{0}$;
- the voltage angle at the reference bus is always zero: $\Delta \theta_{\text{ref}} = 0$.

Rearranging the resulting system of equations allows us to define the changes in all variables of interest (i.e., $\Delta \mathbf{y} \setminus \{\Delta \mathbf{P}_{\text{PV}}, \Delta \mathbf{P}_{\text{PQ}}, \Delta \mathbf{Q}_{\text{PQ}}, \Delta \mathbf{u}_{\text{PV}}, \Delta u_{\text{ref}}, \Delta \theta_{\text{ref}}\}$) as a function of ξ . The changes in active and reactive branch flows due to fluctuations in wind infeed can be represented by a linear combination of the changes in u , c and s variables, as shown in Eq. (17) for active branch flows.

$$\Delta P_{ij}(\xi) = -G_{ij}\Delta u_i + G_{ij}\Delta c_l - B_{ij}\Delta s_l, \quad \forall l \in \mathcal{L}. \quad (17)$$

The chance constraints of the apparent branch flow constraints are thus formulated as quadratic chance constraints for all lines $l := (i, j)$ (and analogously for the reversed power flow direction (j, i)),

$$\mathbb{P}\left[\left(P_{ij} + \Delta P_{ij}(\xi)\right)^2 + \left(Q_{ij} + \Delta Q_{ij}(\xi)\right)^2 \leq \left(\bar{S}_l\right)^2\right] \geq 1 - \epsilon. \quad (18)$$

3) *Reformulating the Linear Chance Constraints:* The LDR approach coupled with the assumption that the wind deviations ξ follow a multivariate Gaussian distribution with zero mean and known covariance allows us to analytically reformulate the single chance constraints in (15) to deterministic constraints [15]. We choose the analytical approach based on a Gaussian distribution given that previous work in [1] has shown that (a) it is reasonably accurate, even when the uncertainty is not normally distributed, and (b) it performs better than sample-based reformulations based on Monte Carlo simulations and the so-called scenario approach [18]. Using the properties of the Gaussian distribution, the linear chance constraint $\mathbb{P}[\mathbf{y} + \mathbf{Y}\xi \leq \bar{\mathbf{y}}] \geq 1 - \epsilon$ is reformulated as follows:

$$\mathbf{y} + \Phi^{-1}(1 - \epsilon)\sqrt{\mathbf{Y}\Sigma\mathbf{Y}^T} \leq \bar{\mathbf{y}}, \quad (19)$$

where Φ^{-1} and Σ denote the inverse cumulative distribution function of the Gaussian distribution and the $(|\mathcal{N}| \times |\mathcal{N}|)$ covariance matrix, respectively. Note that \mathbf{Y} is a $(1 \times |\mathcal{N}|)$ vector containing the sensitivity of the considered variable w.r.t. ξ at each node in \mathcal{W} or 0 at the entries of all other nodes in $\mathcal{N} \setminus \mathcal{W}$. It can be observed that introducing uncertainties results in a tightening of the original constraint $\mathbf{y} \leq \bar{\mathbf{y}}$ and thus, a reduction of the feasible space to the CR defined by the confidence level $(1 - \epsilon)$. The introduced margin $\Omega = \Phi^{-1}(1 - \epsilon)\sqrt{\mathbf{Y}\Sigma\mathbf{Y}^T}$ secures the system against uncertain infeeds and was termed *uncertainty margin* in [15].

4) *Reformulating the Quadratic Chance Constraints:* The apparent flow constraint inside (18) is indeed convex but nonlinear, which prevents a straight-forward analytical reformulation of the chance constraint similar to the linear one in (19). We therefore approximate the quadratic chance constraint by a set of probabilistic absolute value constraints and a nonprobabilistic quadratic constraint as proposed in [10]. Constraint (18) is replaced by the following set of constraints:

$$\mathbb{P}\left[|P_{ij} + \Delta P_{ij}(\xi)| \leq k_{ij}^P\right] \geq 1 - \beta\epsilon, \quad (20)$$

$$\mathbb{P}\left[|Q_{ij} + \Delta Q_{ij}(\xi)| \leq k_{ij}^Q\right] \geq 1 - (1 - \beta)\epsilon, \quad (21)$$

$$(k_{ij}^P)^2 + (k_{ij}^Q)^2 \leq (\bar{S}_l)^2. \quad (22)$$

k_{ij}^P and k_{ij}^Q are optimization variables introduced to enable the reformulation. The absolute value constraints (20) and (21), also called two-sided linear chance constraints, are a special type of joint chance constraints and can be approximated by two single linear chance constraints, e.g. $\mathbb{P}[P_{ij} + \Delta P_{ij}(\xi) \leq k_{ij}^P] \geq 1 - \beta\epsilon$ and $\mathbb{P}[P_{ij} + \Delta P_{ij}(\xi) \geq -k_{ij}^P] \geq 1 - \beta\epsilon$. In this form, the constraints can be reformulated analytically as described in Section III-B3. $\beta \in (0, 1)$ is a parameter, which balances the trade-off between violations in the two constraints (20) and (21) and ensures that the union of the constraints still satisfies the desired confidence level, i.e., $\mathbb{P}[(20) \cup (21)] \geq 1 - \epsilon$. Note that without β , i.e., when enforcing (20) and (21) with $(1 - \epsilon)$, respectively, the union $\mathbb{P}[(20) \cup (21)]$ only holds with $(1 - 2\epsilon)$ [10].

5) *Modeling Inaccuracies:* The linearization of the uncertainty impact and the approximation of the quadratic chance constraints are sources of inaccuracies and entail that the CC-SOC-OPF might still be a strict relaxation of the AC-OPF and the CR (i.e., the chance-constrained AC-OPF) despite the constraint tightenings as depicted in Fig. 2. This highlights the need for appropriate back-mapping procedures to project the CC-SOC-OPF solution back into the feasible space through either ex ante relaxation tightenings or an ex post power flow analysis. Tightenings improve the relaxation but can still not guarantee AC feasibility of the solution. Therefore, we propose to use the solution of the relaxed OPF as a warm start to an AC power flow analysis. To ensure that the CC-SOC-OPF solution is not only projected back into the AC feasible space but into the CR, increased levels of conservatism are required in the CC-SOC-OPF modeling, where β provides an additional degree of freedom to tighten the relaxation along the dimension of the corresponding quadratic chance constraint. Note that the CC-SOC-OPF solution might still not be AC feasible due to loose bounds along other dimensions, but can be made so through the feasibility recovery. How to appropriately choose β has to our knowledge not been addressed in previous work. Performing a rigorous investigation in our case studies, we find that for $\mathbb{P}[(20) \cup (21)] \geq 1 - \epsilon$ to hold while keeping the additional cost incurred by the uncertainty as low as possible, β needs to be tuned for each quadratic chance constraint individually.

6) *Contingency Screening:* In order to reduce both the effort associated with the parameter tuning and the number of new variables and constraints, which need to be introduced to reformulate (18), we propose to perform a contingency screening based on the forecasted operating point. Specifically,

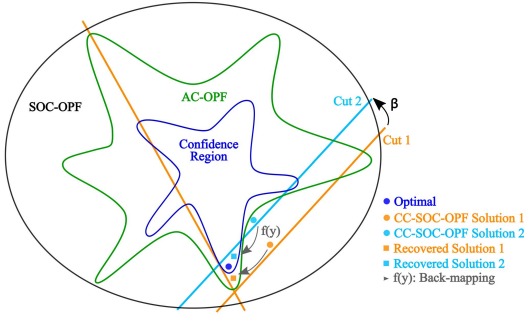


Fig. 2. Illustration of how modeling inaccuracies might affect the CC-SOC-OPF and visualization of the AC feasibility recovery (back-mapping).

we evaluate the vertices κ of the polyhedral outer approximation of the ellipsoidal uncertainty set given by the multivariate Gaussian distribution [4], as one of the vertices includes the worst-case realization of the ellipsoidal uncertainty set. We then use a linearization based on Power Transfer Distribution Factors (PTDF) to approximate the change in active power line flows at each vertex, i.e., $\Delta \mathbf{P}^{\kappa} = \mathbf{PTDF} \times \Delta \mathbf{P}^{\kappa}$, where the change in active power injection $\Delta \mathbf{P}^{\kappa}$ is defined w.r.t. the forecasted operating point. The final active power flows at each vertex show which lines could be overloaded and thus, have a high risk of exceeding the allowable violation probability. These lines are classified as *critical* and their capacity constraints are included as chance constraints. The branch flows on all other lines are constrained by their usual limits and do not consider an uncertainty margin. This procedure takes place iteratively after every solution of a CC-SOC-OPF until no new critical lines are identified.

C. Solution Algorithm

The sensitivity factors Υ depend nonlinearly on the operating point and would render the problem nonconvex if they were introduced as optimization variables. Therefore, we define Υ and the uncertainty margins Ω outside the optimization problem and adopt the iterative solution algorithm from [2] and apply it in the context of a SOC-OPF, which allows us to maintain the convexity of the CC-SOC-OPF. We improve on the work in [2] and [1] by avoiding nonconvexities in the optimization and thus, provide convergence guarantees for the iterative solution algorithm. The algorithm converges as soon as the change in Ω between two consecutive iterations is lower than a pre-defined tolerance value ρ and is defined as follows:

- 1: Set iteration count: $\nu \leftarrow 0$
- 2: **while** $\|\Omega^{\nu} - \Omega^{\nu-1}\|_{\infty} > \rho$ **do**
- 3: **if** $\nu = 0$ **then**
- 4: solve the SOC-OPF for the forecasted wind infeed without considering uncertainty and obtain the operating point \mathbf{y}^0
- 5: evaluate Υ^0 and Ω^0 at \mathbf{y}^0
- 6: **end if**
- 7: perform contingency screening based on \mathbf{y}^{ν} and κ and append the *critical* line list
- 8: include Ω^{ν} according to (19) for all variables $\mathbf{y}(\xi)$ and (20)-(22) for all *critical* lines

- 9: solve CC-SOC-OPF to obtain $\mathbf{y}^{\nu+1}$
- 10: evaluate $\Upsilon^{\nu+1}$ and $\Omega^{\nu+1}$ at $\mathbf{y}^{\nu+1}$
- 11: $\nu \leftarrow \nu + 1$
- 12: **end while.**

This allows us to fully exploit the efficiency of solvers for convex programming. Note that the iterative solution algorithm for the chance constraints adds an additional outer iteration loop to the iterative conic procedure for approximating the angle constraint (5).

IV. CASE STUDY

We evaluate the performance of the proposed CC-SOC-OPF on the IEEE 118 bus test system [19]. We assume the MW line ratings given in [19] as MVA line ratings and reduce them by 30% to obtain a more constrained system. We add wind farms to node 5 and 64 with expected production levels of 300 MW and 600 MW, respectively. We assume a standard deviation of 10% and a power factor between 0.95 capacitive and 0.95 inductive for each wind farm. Minimum and maximum voltage limits are set to 0.94 p.u. and 1.06 p.u.. Generator cost functions are assumed to be linear.

We first demonstrate how a SOC-OPF coupled with an AC feasibility recovery is able to approach the solution of a nonlinear solver for the exact AC-OPF problem. Afterwards, we show how the convex CC-SOC-OPF coupled with the AC feasibility recovery is able to identify even better solutions in terms of operation cost than the CC-AC-OPF from [1]. We evaluate the constraint violation probabilities in all cases empirically using Monte Carlo simulations of AC power flow calculations based on 10'000 scenarios drawn from a multivariate Gaussian distribution. All simulations related to SOC-OPFs were carried out in Python using the Gurobi Optimizer. The nonconvex CC-AC-OPF was implemented in Matlab, where the OPF at each iteration was solved using Matpower and its internal MIPS solver [20]. All AC power flow analyses, i.e., the AC feasibility recovery and the Monte Carlo simulations, were also carried out with Matpower.

A. Recovering the SOC-OPF Solution

We evaluate the SOC-OPF at the forecasted operating point without considering wind power uncertainty and compare the outcome to the standard AC-OPF solution. We assume a convergence tolerance of 10^{-6} for the sequential conic procedure to approximate the angle constraint (5). The objective function value of the relaxed problem is identical to the one obtained with the exact problem (37'692.03€), providing a seemingly tight relaxation with zero relaxation gap. However, when evaluating the full AC power flow equations at the operating point identified by the SOC-OPF, we observe a mismatch of active and reactive power injections at nodes 37 and 38, which despite being fairly small (i.e., 0.06 MW and 0.98 Mvar) indicate that the operating point is not AC feasible. The infeasibility is also reflected in the SOC constraint of line 50 connecting nodes 37 and 38, which is the only one that fails to maintain the equality constraint (4) at the SOC-OPF solution. This also highlights the inadequacy of defining the relaxation gap of OPF relaxations solely based on differences in objective function values. The OPF objective function only

TABLE I

RESULTS OF THE MONTE CARLO SIMULATIONS: COMPARISON OF MAXIMUM VIOLATION PROBABILITIES BETWEEN AC-OPF, SOC-OPF*, CC-SOC-OPF* AND CC-AC-OPF. THE RESULTS OF THE CC-SOC-OPF* INCLUDE THE ONES OBTAINED WITHOUT β AND WITH THE FINAL OPTIMAL VALUES FOR β .

AC-OPF	SOC-OPF*	CC-AC-OPF	CC-SOC-OPF*	
			$\beta = \emptyset$	$\beta \neq \emptyset$
Generator active power limits				
48.74%	48.74%	5.00%	4.96%	4.96%
Bus voltage limits				
43.86%	56.89%	3.26%	1.30%	0.25%
Apparent power line flow limits				
50.22%	50.12%	4.07%	7.72%	5.00%
Joint violation probability				
100%	100%	14.85%	17.35%	15.60%

* The Monte Carlo simulations were carried out with the recovered SOC solution.

considers costs on active power generation and thus, neglects the fact that one \mathbf{P} solution might be associated with numerous $\{\mathbf{Q}, \mathbf{V}, \theta\}$ solutions, not all of which might be feasible.

Therefore, we propose to use the SOC-OPF solution as a warm start to an AC power flow analysis in order to recover the feasible AC power flow solution. Similar to the tolerance for evaluating the results of the Monte Carlo simulation, we consider a tolerance of 0.1% for this procedure to exclude numerical errors. Given that power flow calculations do not consider any variable limits, we need to enforce generator reactive power limits, and slack bus active power limits (by e.g. changing the slack bus if necessary), and check for voltage and branch flow limits. The final power flow solution results in a dispatch with slightly lower generation cost (37'691.97€), which is due to the considered tolerance.

The results of the Monte Carlo simulations are listed in Table I showing the maximum violation probabilities for generator active power, bus voltage, and apparent branch flow limits. Table I also shows the joint violation probability, which represents the probability of at least one constraint being violated (i.e., the number of samples with at least one constraint violation out of the 10'000 tested). A joint violation probability of 100% for the standard AC-OPF and SOC-OPF indicates that neither OPF algorithm results in an operating point, which is able to maintain feasibility for any other wind power realization if uncertainty in wind power infeed is not explicitly accounted for. The maximum violation probability of single constraints in that case lies around 50%.

B. Contingency Screening

The contingency screening shows that line 100, which is already congested at \mathbf{y}^0 , violates its branch flow limits in both directions of the line. Furthermore, the limits of line 37, which is not congested at \mathbf{y}^0 , are also estimated to be violated in the positive flow direction (i.e., from node 8 to node 30). Thus, we include three quadratic chance constraints: two for line 100 defining both flow directions and one for line 37 defining only the positive flow direction. The weighting factors are denoted with $\beta_{100}^{\rightarrow}$ and β_{37}^{\rightarrow} with the arrows indicating the direction of the constrained flow.

C. Chance-constrained SOC-OPF

We first determine the optimal parameters β for the CC-SOC-OPF and then compare it to the CC-AC-OPF algorithm proposed in [1]. We assume an acceptable violation probability ϵ of 5% for all chance constraints. The convergence tolerance ρ of the uncertainty margins for the iterative CC-SOC-OPF and CC-AC-OPF is set to 10^{-5} . Both algorithms converge after 4 iterations demonstrating the suitability of the iterative solution algorithm for both OPFs. However, the algorithm is more robust in case of the SOC-OPF due to the convexity of the problem solved at each iteration step, which provides convergence guarantees [21].

1) *Quadratic chance constraints without weighting factors* $\beta = \emptyset$: First, we analyze the solution without considering the weighting factors $\beta_{100}^{\rightarrow}$ and β_{37}^{\rightarrow} , i.e., we enforce the two separate absolute value constraints (20)-(21) for each quadratic chance constraint with the usual confidence level $(1 - \epsilon)$. The results are listed in Table I. It can be observed that the chance constraints for active power generation and voltage magnitudes are satisfied. However, the maximum violation probability of the apparent branch flow limits exceeds the allowable threshold of 5% and indicate that the recovered solution is not located within the CR. Specifically, this violation is caused by the flow in the positive flow direction on line 37 and confirms that the union of the two separate constraints (20) and (21) only holds with $1 - 2\epsilon$ as described in Section III-B4. In case of line 100, the level of conservatism for enforcing the two separate constraints is already sufficient, such that the violation probabilities are reduced to 4.47% and 4.17% in the positive and negative flow directions, respectively.

2) *Quadratic chance constraints with weighting factors* $\beta = \{\beta_{37}^{\rightarrow}, \beta_{100}^{\rightarrow}\}$: In order to evaluate the impact of different values of the weighting factors on the CC-SOC-OPF, we perform a sensitivity analysis varying $\beta_{100}^{\rightarrow}$ uniformly in both flow directions from 0.1 to 0.9 in 0.1 increments and add 0.01 and 0.99 as the approximate endpoints of the interval $\beta \in (0, 1)$ (i.e., in total 11 samples). As line 37 has proven to be more critical, we use a finer sampling of β_{37}^{\rightarrow} between 0.02 and 0.98 in 0.02 increments (i.e., 49 samples). Hence, we perform the sensitivity analysis based on 539 simulations of the CC-SOC-OPF with a subsequent AC feasibility recovery.

The performance of the resulting 539 operating points when subjected to wind infeed variations is evaluated through Monte Carlo simulations based on 2'000 samples drawn from a Gaussian distribution. The results are visualized in Fig. 3. The top plot shows the maximum violation probability of the apparent branch flow constraints, which in all 539 cases is due to the flow on line 37. It can be seen that lower values of β_{37}^{\rightarrow} and $\beta_{100}^{\rightarrow}$ increase the level of conservatism and reduce the violation probability. β_{37}^{\rightarrow} needs to be lower than approximately 0.6 to keep the violation probability within acceptable levels (i.e. $< 5\%$), while for $\beta_{37}^{\rightarrow} > 0.4$ variations in $\beta_{100}^{\rightarrow}$ do not significantly influence the maximum violation probability. The middle and bottom plots depict the changes in generation cost of the CC-SOC-OPF z^{CC-SOC} and the recovered solution $z^{rCC-SOC}$, respectively. The behavior of the cost development in both cases is similar and leads to an increase in cost with lower weights. Somewhat counter-intuitive though, the cost of the recovered AC feasible solution $z^{rCC-SOC}$ is

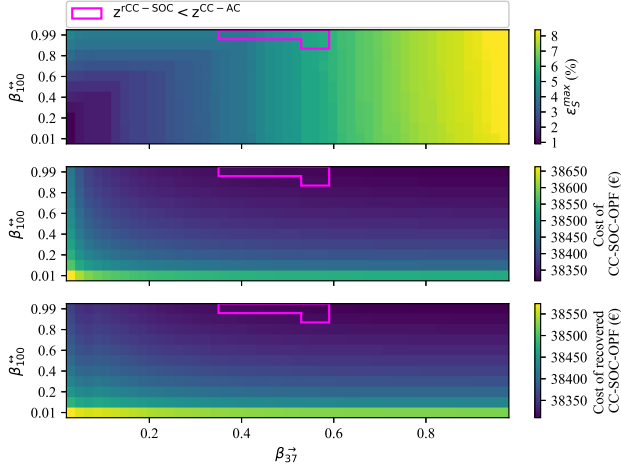


Fig. 3. Maximum violation probability of apparent branch flows ϵ_S^{max} , generation cost of the CC-SOC-OPF (z^{CC-SOC}) and the recovered CC-SOC-OPF solution (z^{CC-SOC}) as functions of β_{37} and β_{100} . The pink box indicates the region of operating points, which are located inside the CR and are cheaper than the benchmark CC-AC-OPF solution.

lower than the cost of the CC-SOC-OPF z^{CC-SOC} . This is a consequence of the approximation of the chance constraints in order to make them tractable. As shown in the illustration of “cut 2” in Fig. 2, the linear cuts lead to some parts of the AC feasible space being cut off and not represented in the CC-SOC-OPF. Our feasibility recovery procedure however, not constrained by those linear cuts, is able to determine solutions inside the confidence region, which can have lower costs.

We use a finer sampling of β_{37} between 0.5 and 0.6 and evaluate the resulting operating points with 10^4 Monte Carlo simulations to determine its optimal value, which complies with the maximum violation probability but does not lead to unnecessarily high levels of conservatism and cost. We do not assume any weights for the chance constraints associated with line 100, as they are already met when enforced with the usual confidence level. Fig. 4 depicts the change in violation probabilities and cost for the finer sampling. A value of 0.555 for β_{37} has proven to just meet the maximum allowable 5% violation probability while still leading to lower operation cost at its recovered solution than the CC-AC-OPF.

3) *Comparison with CC-AC-OPF*: The CC-SOC-OPF coupled with the AC feasibility recovery results in an operating point with lower cost as shown in Table II and is thus, less conservative. This is also reflected in less conservative violation probabilities shown in Table I. The weights β on the quadratic chance constraints provide a significant additional degree of freedom in the CC-SOC-OPF, which can be used to, e.g., reduce the joint violation probability of the original OPF and increase its robustness without the need to explicitly account for joint chance constraints and use computationally demanding sample-based scenario approaches to reformulate them. In this case study, joint violation probabilities of less than 10% can be achieved as depicted in Fig. 5.

The pink box in Fig. 3 highlights the recovered solutions of the CC-SOC-OPF, which are located within the CR and have lower generation cost z^{CC-SOC} than the CC-AC-OPF z^{CC-AC} . Apart from the operating points depicted in the

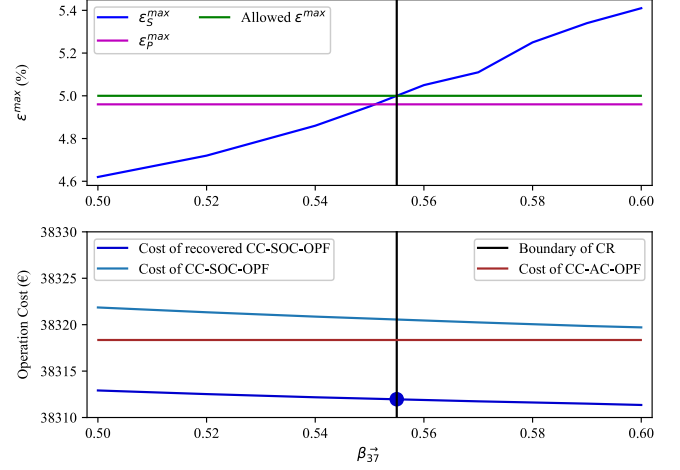


Fig. 4. Operation cost and maximum violation probability of apparent branch flow ϵ_S^{max} and active power generation ϵ_P^{max} limits for different values of β_{37} along line 37 and a constant confidence level $(1 - \epsilon)$ for the quadratic chance constraints associated with line 100.

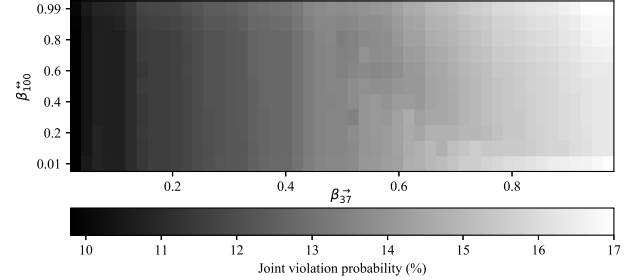


Fig. 5. Joint violation probability for different values of β_{37} and β_{100} .

pink box, 10 other ones identified during the finer sampling of β_{37} (i.e., $0.5 \leq \beta_{37} \leq 0.6$) also fulfill the original chance constraints and outperform the CC-AC-OPF in terms of operation cost. Thus, apart from the least-cost solution listed in Table I and II, we find 18 other operating points, which are AC feasible, fulfill the original chance constraints and are still cheaper than the CC-AC-OPF solution of the nonlinear solver. This highlights (a) the potential of convex relaxations to determine the boundaries of the CR and the true optimal of nonconvex problems, and (b) the importance of appropriate back-mapping procedures to translate the solution of the convex approximation back to the original domain. Despite the required tuning, β provides the flexibility to vary the shape of the convex approximation and direct the solution from a true lower bound back into the original feasible space and the CR.

TABLE II
COMPARISON OF CC-AC-OPF AND CC-SOC-OPF*.

	CC-AC-OPF	CC-SOC-OPF*
Cost	38'318.35 €	38'311.12 €
Iterations	4	4
Time	4.42 s	10.60 s

* Refers to the recovered SOC solution.

The need for computationally more efficient convex relaxations of (chance-constrained) AC-OPFs was identified in [4], where we developed a SDP relaxation of the chance-constrained AC-OPF based on rectangular and Gaussian uncertainty sets. Comparable instances to our case study may take up to 10 minutes to solve with the SDP relaxation (although the computational improvements proposed in [22] can reduce this time) whereas our proposed algorithm converges within 10.60 s. The CC-AC-OPF converges even faster after only 4.42 s. The solution time of the CC-SOC-OPF is mainly determined by the inner iteration loop for approximating the angle constraint (5), which accounts for 84% of the total solution time. More efficient approximations of the angle constraint, which can be implemented in a one-shot optimization, could significantly improve the performance of the proposed method. Still, the combination of the iterative algorithm and convex programming makes the method already computationally very efficient and robust, and suitable for large-scale systems as demonstrated in our case study.

V. CONCLUSION

This paper deals with the impact of linear approximations for the unknown nonconvex confidence region of chance-constrained AC-OPF problems.

In that, we introduce the first formulation of a chance-constrained second-order cone OPF. Our approach is superior to existing approaches, as it defines a convex problem and thus, provides convergence guarantees, while it is computationally more efficient than other convex relaxation approaches. Coupled with an AC feasibility recovery, we show that it can determine better solutions than nonconvex chance-constrained AC-OPF formulations.

To the best of our knowledge, this is the first paper that performs a rigorous analysis of the AC feasibility recovery for robust SOC-OPF formulations. Due to the SOC relaxation, a CC-SOC-OPF might determine AC infeasible operating points, while the linear reformulations of the chance constraints result in solutions, which either lie outside the confidence region or are too conservative. Inaccurate approximations of the confidence region is an issue for all chance-constrained AC-OPF formulations. In this paper, we introduce an approximation of the quadratic apparent power flow chance constraints with linear chance constraints using results proposed in [10]. Through that, we introduce new parameters able to reshape the approximation of the confidence region, offering a high degree of flexibility.

Our paper shows that further work on better and computationally more efficient approximations for the chance-constrained AC-OPF problem is necessary. In future work, we are planning to use a combination of data-driven methods [23] and convex relaxations to develop a scalable approach to chance-constrained OPFs with a more accurate representation of the confidence region, as our previous work in [24] has shown how nonconvex feasible spaces of AC-OPFs can be efficiently incorporated in a convex optimization framework using convex subspaces and mixed-integer second-order cone programming.

REFERENCES

- [1] L. Roald and G. Andersson, "Chance-Constrained AC Optimal Power Flow: Reformulations and Efficient Algorithms," *IEEE Transactions on Power Systems*, vol. PP, no. 99, pp. 1–1, 2017.
- [2] J. Schmidli, L. Roald, S. Chatzivasileiadis, and G. Andersson, "Stochastic AC Optimal Power Flow with Approximate Chance-Constraints," in *2016 IEEE Power and Energy Society General Meeting (PESGM)*, July 2016, pp. 1–5.
- [3] H. Zhang and P. Li, "Chance Constrained Programming for Optimal Power Flow Under Uncertainty," *IEEE Transactions on Power Systems*, vol. 26, no. 4, pp. 2417–2424, Nov 2011.
- [4] A. Venzke, L. Halilbasic, U. Markovic, G. Hug, and S. Chatzivasileiadis, "Convex Relaxations of Chance Constrained AC Optimal Power Flow," *IEEE Transactions on Power Systems*, 2017, (in press).
- [5] B. Kocuk, S. S. Dey, and X. A. Sun, "Strong SOCP Relaxations for the Optimal Power Flow Problem," *Operations Research*, vol. 64, no. 6, pp. 1177–1196, 2016.
- [6] A. Lorca and X. A. Sun, "The Adaptive Robust Multi-Period Alternating Current Optimal Power Flow Problem," *IEEE Transactions on Power Systems*, vol. 33, no. 2, pp. 1993–2003, March 2018.
- [7] X. Bai, L. Qu, and W. Qiao, "Robust AC Optimal Power Flow for Power Networks With Wind Power Generation," *IEEE Transactions on Power Systems*, vol. 31, no. 5, pp. 4163–4164, Sept 2016.
- [8] Y. Zhou, Y. Tian, K. Wang, and M. Ghandhari, "Robust Optimisation for AC-DC Power Flow based on Second-Order Cone Programming," *The Journal of Engineering*, vol. 2017, no. 13, pp. 2164–2167, 2017.
- [9] R. A. Jabr, "Adjustable Robust OPF With Renewable Energy Sources," *IEEE Transactions on Power Systems*, vol. 28, no. 4, pp. 4742–4751, Nov 2013.
- [10] M. Lubin, D. Bienstock, and J. P. Vielma, "Two-sided Linear Chance Constraints and Extensions," *ArXiv e-prints*, Jul. 2015.
- [11] M. B. Cain, R. P. O'Neill, and A. Castillo, "History of Optimal Power Flow and Formulations - Optimal Power Flow Paper 1," 2012. [Online]. Available: <https://www.ferc.gov/industries/electric/indus-act/market-planning/opf-papers/acopf-1-history-formulation-testing.pdf>
- [12] A. G. Esposito and E. R. Ramos, "Reliable Load Flow Technique for Radial Distribution Networks," *IEEE Transactions on Power Systems*, vol. 14, no. 3, pp. 1063–1069, Aug 1999.
- [13] R. A. Jabr, "A Conic Quadratic Format for the Load Flow Equations of Meshed Networks," *IEEE Transactions on Power Systems*, vol. 22, no. 4, pp. 2285–2286, Nov 2007.
- [14] M. Tsili and S. Papathanassiou, "A Review of Grid Code Technical Requirements for Wind Farms," *IET Renewable Power Generation*, vol. 3, no. 3, pp. 308–332, Sept 2009.
- [15] L. Roald, F. Oldewurtel, T. Krause, and G. Andersson, "Analytical Reformulation of Security Constrained Optimal Power Flow with Probabilistic Constraints," in *2013 IEEE PowerTech Grenoble Conference*, June 2013.
- [16] H. Qu, L. Roald, and G. Andersson, "Uncertainty Margins for Probabilistic AC Security Assessment," in *2015 IEEE Eindhoven PowerTech*, June 2015, pp. 1–6.
- [17] L. Roald, "Optimization Methods to Manage Uncertainty and Risk in Power System Operation," Ph.D. dissertation, ETH Zurich, 2016.
- [18] K. Margellos, P. Goulart, and J. Lygeros, "On the Road Between Robust Optimization and the Scenario Approach for Chance Constrained Optimization Problems," *IEEE Transactions on Automatic Control*, vol. 59, no. 8, pp. 2258–2263, Aug 2014.
- [19] "IEEE 118-bus, 54-unit, 24-hour system," Electrical and Computer Engineering Department, Illinois Institute of Technology, Tech. Rep. [Online]. Available: http://motor.ece.iit.edu/data/JEAS_IEEE118.doc
- [20] R. D. Zimmerman, C. E. Murillo-Sanchez, and R. J. Thomas, "MATPOWER: Steady-State Operations, Planning, and Analysis Tools for Power Systems Research and Education," *IEEE Transactions on Power Systems*, vol. 26, no. 1, pp. 12–19, Feb 2011.
- [21] A. J. Conejo, E. Castillo, R. Mínguez, and R. García-Bertrand, *Decomposition Techniques in Mathematical Programming: Engineering and Science Applications*. Springer-Verlag, 2006.
- [22] A. Venzke and S. Chatzivasileiadis, "Convex Relaxations of Security Constrained AC Optimal Power Flow under Uncertainty," in *Power Systems Computation Conference (PSCC) 2018*, June 2018.
- [23] F. Thams, L. Halilbašić, P. Pinson, S. Chatzivasileiadis, and R. Eriksson, "Data-Driven Security-Constrained OPF," *10th IREP Symposium - Bulk Power Systems Dynamics and Control*, 2017.
- [24] L. Halilbašić, F. Thams, A. Venzke, S. Chatzivasileiadis, and P. Pinson, "Data-driven Security-Constrained AC-OPF for Operations and Markets," in *Power Systems Computation Conference (PSCC) 2018*, June 2018.